arXiv:1603.00451v2 [cond-mat.quant-gas] 14 Feb 2017

In-commensurate Skyrmion crystals, devil staircases and multi-fractals due to spin orbit coupling in a lattice system

Fadi Sun[1,2,3] and Jinwu Ye [1,2,3]
[1] *Department of Physics and Astronomy, Mississippi State University, MS, 39762, USA*
[2] *Department of Physics, Capital Normal University, Key Laboratory of Terahertz Optoelectronics, Ministry of Education, and Beijing Advanced innovation Center for Imaging Technology, Beijing, 100048, China*
[3] *Kavli Institute of Theoretical Physics, University of California, Santa Barbara, Santa Barbara, CA 93106*

(Dated: February 15, 2017)

In this advance, we study the system of strongly interacting spinor bosons in a square lattice subject to any of the linear combinations of the Rashba and Dresselhaus spin-orbit coupling (SOC). The SOC leads to novel and rich quantum and topological phenomena in a lattice system. They include masses generated from "order from quantum disorder " mechanism, collinear spin-bond correlated magnetic phase, quantum commensurate (C) and In-commensurate (IC) non-coplanar Skyrmion crystal phases, stripe co-planar (spiral) C and IC phases, quantum Lifshitz C-IC transitions, metastable states, hysteresis, topological rational and irrational winding numbers, incomplete and complete devil staircases, Cantor sets, multi-fractals, etc. Various perspectives and possible intimate connections with topological spin liquids due to geometric frustrations or quantum spin glass due to quenched disorders are discussed. Implications on current or near future cold atom systems and on 4d or 5d strongly correlated materials with SOC are discussed.

INTRODUCTION. It was well known that the strong correlations among bosons or fermions lead to many quantum, topological phases and phase transitions in materials[1–3]. Its combinations with geometric frustrations may lead to new phases of matter such as coplanar spiral phases, especially topological quantum spin liquids[2–5]. Its combinations with quenched disorders also lead to new states of matter such as the quantum spin glass[6–9] which is closely related to black hole physics through AdS/CFT correspondences[10–14]. On the other forefront, Rashba or Dresselhaus spin-orbit coupling (SOC) is ubiquitous in various 2d or layered non-centrosymmetric insulators, semi-conductor systems, metals and superconductors[15–22]. There are also recent remarkable experimental advances in generating any linear combinations of the 2d Rashba and Dresselhaus SOC for both fermions and spinor bosons in both continuum and optical lattices[23–30]. New many body phenomena due to the interplay among strong interactions, the SOC and lattice geometries are being investigated in the current cold atom experiments. It becomes urgent, topical and important to investigate what would be the new quantum or topological phenomena due to the the interplay between the strong correlations and the ubiquitous Rashba or Dresselhaus SOC on various lattices.

In this work, we address this outstanding problem and discover that the interplay leads to many novel quantum or topological phenomena summarized in the global quantum phase diagram Fig.1. They include masses generated from "order from quantum disorder " phenomena, the collinear spin-bond correlated Y-x phase and its novel excitation spectrum, quantum commensurate (C) and In-commensurate (IC) non-coplanar Skyrmion crystal (SkX) phases, stripe co-planar (spiral) C and IC phases, quantum Lifshitz C-IC transitions, metastable states, hysteresis, topological fractional and irrational winding numbers, incomplete and complete devil staircases, Cantor sets, multi-fractals, etc. We establish the Fig.1 by the combinations of the approaches from the extremely anisotropic limit[32] ($\alpha = \pi/2, \beta$), the isotropic Rashba limit $0 < \alpha = \beta < \pi/2$ and near the Abelian line $0 < \alpha < \pi/2, \beta = 0$. Our results demonstrate that the interplay among strong correlations, Rashba SOC and lattice geometries opens a new avenue to explore whole new classes of quantum or topological phenomena which may have wide implications in cold atoms and various materials with SOC to be discussed near to the end of the paper.

The tight-binding Hamiltonian of (pseudo)-spin 1/2 bosons (or fermions) at integer (or half) fillings hopping in a two-dimensional square optical lattice subject to any combination of Rashba and Dresselhaus SOC is:

$$\mathcal{H}_{b/f} = -t\sum_{\langle ij\rangle}(b^{\dagger}_{i\sigma}U^{\sigma\sigma'}_{ij}b_{j\sigma'} + h.c.) + \frac{U}{2}\sum_{i}(n_i - N)^2 \quad (1)$$

where t is the hopping amplitude along the nearest neighbors $\langle ij\rangle$, the non-Abelian gauge fields $U_{ii+\hat{x}} = e^{i\alpha\sigma_x}$, $U_{ii+\hat{y}} = e^{i\beta\sigma_y}$ are put on the two links in a square lattice. $\alpha = \pm\beta$ stands for the Rashba (Dresselhaus) case. $\alpha \neq \beta$ corresponds to any linear combination of the two. $U > 0$ is the Hubbard onsite interaction.

In the strong coupling limit $U/t \gg 1$, to the order $O(t^2/U)$, we obtain the effective spin $s = N/2$ Rotated Heisenberg model:

$$\mathcal{H}_{RH} = -J\sum_{i}[\mathbf{S}_i R(\hat{x}, 2\alpha)\mathbf{S}_{i+\hat{x}} + \mathbf{S}_i R(\hat{y}, 2\beta)\mathbf{S}_{i+\hat{y}}] \quad (2)$$

with $J = \pm 4t^2/U > 0$ for bosons/fermions, the $R(\hat{x}, 2\alpha)$, $R(\hat{y}, 2\beta)$ are the two SO(3) rotation matrices around the X and Y spin axis by angle 2α, 2β putting on the two

bonds along $\hat{x}$, $\hat{y}$ respectively. In this paper, for simplicity, we first focus on spinor bosons. The fermions will be discussed in a separate publication.

The RFHM Eq.2 at a generic (α, β) has the translational, the time reversal $\mathcal{T}$, the three spin-orbital coupled Z_2 symmetries $\mathcal{P}_x, \mathcal{P}_y, \mathcal{P}_z$ symmetries[32]. Along the extremely anisotropic limit $\alpha = \pi/2, 0 < \beta < \pi/2$, there is a hidden spin-orbital coupled $U(1)$ symmetry generated by $U_1(\phi) = e^{i\phi \sum_i (-1)^x S_i^z}$ and also the Mirror symmetry $\mathcal{M}$ which consists of the local rotation $\tilde{\mathbf{S}}_i = R(\hat{x}, \pi) R(\hat{z}, \pi n_2) \mathbf{S}_i$ followed by a Time reversal transformation $\mathcal{T}$, $(\beta, h) \to (\pi/2 - \beta, h)$. However, any deviation from the extremely anisotropic line $\alpha \neq \pi/2$ spoils the $U(1)$ and Mirror symmetry. Along the isotropic Rashba limit $\alpha = \beta$, the $\mathcal{P}_z$ symmetry is enlarged to the spin-orbital coupled $C_4 \times C_4$ symmetry around the z axis. Of course, along the bottom Abelian line $0 < \alpha < \pi/2, \beta = 0$, it has the $\tilde{SU}(2)$ symmetry in the $\tilde{SU}(2)$ basis $\tilde{\mathbf{S}}_n = R(\hat{x}, 2\alpha n)\mathbf{S}_n$. Because $\beta < \alpha$ lower-half is related to the $\beta > \alpha$ upper half in Fig.1 by the $C_4 \times C_4$ transformation, so in the following, we mainly focus on the lower half. We will approach the global phase diagram Fig.1 from all the three lines: the solvable line $\alpha = \pi/2, 0 < \beta < \pi/2$, the Abelian line $0 < \alpha < \pi/2, \beta = 0$ and the diagonal line $0 < \alpha = \beta < \pi/2$.

RESULTS

C and IC Magnons in the Y-x state and their condensations. The firmly established results and physical insights[32] achieved on the extremely anisotropic line $(\alpha = \pi/2, \alpha < \beta)$ pave the way to study the physics at generic (α, β) in Fig.1. Especially, we will follow how the three kinds of magnons response and evolve when moving away from the line.

Making a globe rotation $R_x(\pi/2)$ to align spin along the Z-axis and then introducing Holstein-Primakoff bosons a and b for the two sublattice, we can expand the Hamiltonian in the powers of $1/\sqrt{S}$,

$$H = E_0 + 2JS\Big[H_2 + \Big(\frac{1}{\sqrt{S}}\Big)H_3 + \Big(\frac{1}{\sqrt{S}}\Big)^2 H_4 + \cdots\Big] \tag{3}$$

where the symbol H_n denotes the n-th polynomial of the boson operators, $E_0 = -2NJS^2 \sin^2\alpha$ is the classical ground state energy of the Y-x state. Performing a unitary transformation, then a Bogoliubov transformation on H_2, one can diagonize H_2 as:

$$H_2 = E_2 + 2\sum_k (\omega_k^+ \alpha_k^\dagger \alpha_k + \omega_k^- \beta_k^\dagger \beta_k) \tag{4}$$

where $E_2 = \sum_k (\omega_k^+ + \omega_k^- - 2\sin^2\alpha)$ is the quantum correction to the ground state energy at the LSW order, $\omega_k^\pm = \sqrt{(\lambda_k^\pm)^2 - \chi_k^2}$, $\lambda_k^\pm = \sin^2\alpha - \frac{1}{2}\cos 2\beta \cos k_y \pm \frac{1}{2}\sqrt{\sin^4\alpha \cos^2 k_x + \sin^2 2\beta \sin^2 k_y}$, $\chi_k = \frac{1}{2}\cos^2\alpha \cos k_x$. Obviously, $\omega_k^\pm = \omega_{-k}^\pm$ which is dictated by the symmetries of the Hamiltonian and the Y-x state. Note that to the LSW order, the dispersion still has the Mirror symmetry under the $\beta \to \pi/2 - \beta$. However the mirror symmetry will be spoiled by the higher order terms starting at H_3.

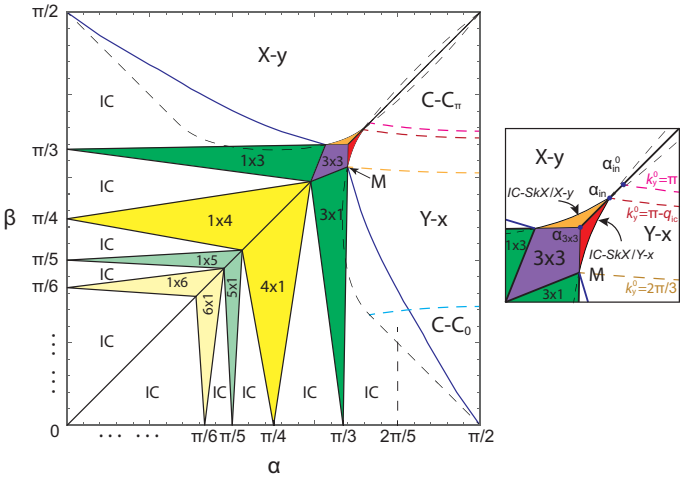

FIG. 1. Phase diagram of the strongly interacting spinor bosons at a generic SOC (α, β) in a square lattice. Along the diagonal line $\alpha_{in} < \alpha < \pi/2$, there is a gap opening generated by the order from disorder mechanism. There is a quantum Lifshitz transition at $\alpha = \alpha_{in}$ with the dynamic exponent $z = 1$, from the collinear Y-x (or X-y) phase to the non-coplanar IC-SkX/Y-x (or IC-SkX/X-y) phase, then a second one from the IC-SkX/Y-x to the commensurate 3×3 SkX crystal phase at $\alpha = \alpha_{33}$ which is a bi-critical point. The segment $\alpha_{33} < \alpha < \alpha_{in}$ is the first order transition line between the IC-SkX/Y-x and IC-SkX/X-y. All the other segments are first order transition lines between $N \times 1$ and $1 \times N$ co-planar spiral phase after $N \geq 4$. M is the multicritical point located at (α_M, β_M) where the $(0, \pm 2\pi/3)$ counter line of the Y-x phase hits the corner of the 3×3 SkX crystal. There is a second order transition from the Y-x phase to the non-coplanar IC-SkX/Y-x phase driven by the condensations of C-IC with $\pi - \pi/3 < k_y^0 < \pi - q_{ic}$. The Y-x state becomes metastable between the first order transition line and the second order transition (dashed) line due to the condensations of the $C - C_0$ and C-IC with $0 < k_y^0 < 2\pi/3$. The in-complete devil's staircases at a small $\beta < \alpha = \pi(1/2, 1/3, 1/4, ...) = \pi/N$ stand for commensurate stripe co-planar spiral phases. The IC means the stripe co-planar in-commensurate phases. Immersed inside the IC phase are some small devil staircases (such as at $3\pi/7, 2\pi/5, 2\pi/7$.....) displaying fractal structures. The relevant numbers are $\alpha_{in}^0 \sim 0.3611\pi, \alpha_{ic} \sim 0.3526\pi, \alpha_{33} \sim 0.3402\pi, (\alpha_M, \beta_M) \sim (0.33952\pi, 0.31284\pi)$ and $q_{ic} \sim 0.18\pi$.

As shown in[32], at $\alpha = \pi/2$, the Y-x state is the exact ground state, $\chi_k = 0$, there is no need for the extra Bogoliubov transformation, the spin wave dispersion reduces to $\omega_k^\pm = \lambda_k^\pm$. As shown in[38], any transverse field h_x or h_z transfers the Y-x state into a co-planar canted state. In sharp contrast, here, under $\pi/2 - \alpha \neq 0$, the Y-x state remains the classical state, but not the exact eigenstate anymore due to the quantum fluctuations introduced by $\alpha \neq \pi/2$. From ω_k^-, one can identify the minimum $(0, k_y^0)$ of spin-wave dispersion corresponding to the magnons C-C_0, C-IC, C-C_π respectively (See SM

). Near $(0, k_y^0)$, their dispersions take the relativistic form:

$$\omega_-(q) = \sqrt{\Delta^2 + v_x^2 q_x^2 + v_y^2 q_y^2} \tag{5}$$

The gap and the two velocities are given in the SM.

The Staggered magnetization and specific heat of the Y-x phase at $T \ll \Delta$ are:

$$M(T) \sim M(T=0) - \frac{T\Delta}{2\pi v_x v_y}\sqrt{1+\frac{\cos^4\alpha}{4\Delta^2}}e^{-\Delta/T}$$
$$C(T) \sim \frac{1}{2\pi v_x v_y}\frac{\Delta^3}{T}e^{-\Delta/T} \tag{6}$$

where $M(T=0) = S - \frac{1}{N}\sum_k(\frac{\lambda_k^+}{2\omega_k^+}+\frac{\lambda_k^-}{2\omega_k^-}-1)$ is the $T=0$ magnetization. At $\alpha = \pi/2$, replacing v_x by $\sqrt{\Delta/m_x}$ and v_y by $\sqrt{\Delta/m_y}$, Eqn.6 gives back to those along the solvable line in[32].

Solving $\Delta = 0$ leads to the 3 segments of their condensation boundary:

$$\alpha = \begin{cases} \pi/2-\beta, \\ \arcsin\left[\frac{\sqrt{6}\sin 2\beta}{\sqrt{9\sin^2 2\beta - 1}}\right], \\ \beta, \end{cases} \tag{7}$$

for $0 \le \beta \le \pi/2 - \arccos(1/\sqrt{6}), \pi/2 - \arccos(1/\sqrt{6}) \le \beta \le \arccos(1/\sqrt{6})$ and $\arccos(1/\sqrt{6}) \le \beta \le \pi/2$ respectively. At the LSW order, it still has the mirror symmetry under $\beta \to \pi/2 - \beta$.

The C-C_π magnons condense along the diagonal line $\arccos(1/\sqrt{6}) \le \beta \le \pi/2$ with the gapless relativistic dispersion:

$$\omega_-(q) = \sqrt{v_x^2 q_x^2 + v_y^2 q_y^2} \tag{8}$$

where $v_x = \cos(\alpha)/2$, $v_y = \cos(\alpha)\sqrt{1-6\cos^2(\alpha)}/2$. Obviously, both velocities vanish at the Abelian point $\alpha = \pi/2, \beta = \pi/2$ dictated by the enlarged $SU(2)$ symmetry. Moving away from the diagonal line $\alpha = \beta$, v_x keeps increasing, but v_y increases first, reaches a maximum, then vanishes at the boundary between C-C_π and C-IC magnons $\alpha_{ic}^0 = arccos(1/\sqrt{6}) \sim 0.36614\pi$. When pushing to higher orders, $\omega_-(q) = \sqrt{v_x^2 q_x^2 + v_y^2 q_y^2 + u^2 q_y^4 + \cdots}$, we find it is a putative ($z_x = 1, z_y = 2$) quantum Lifshitz transition from the Y-x state to an incommensurate state (Fig.4a). However, as to be shown below, the gapless mode along the diagonal line and the mirror symmetry under $\beta \to \pi/2 - \beta$ are just spurious facts of the LSW approximation. However, the quantum Lifshitz transition remains, but with a different dynamic exponent than ($z_x = 1, z_y = 2$).

Order from disorder along the diagonal line near the $\alpha = \beta = \pi/2$ Abelian point. It is important to understand what is the true quantum ground state along the diagonal line near the Abelian point

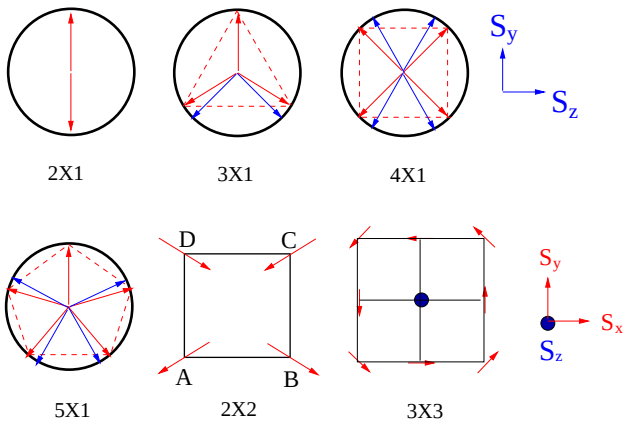

FIG. 2. Some most robust Collinear, spiral, vortex and non-coplanar states in Fig.1. Top layer: the 2×1 (Y-x) state $S^y = (-1)^x$ is the exact quantum ground state[32] at $\alpha = \pi/2$. When β is small, the 3×1 spiral state is close to be a FM state in the rotated basis $\tilde{\mathbf{S}}_n = R(\hat{x}, 2\alpha n)\mathbf{S}_n$. All the red arrows in 120° structure (connected by the dashed line) will be transformed to a FM state in the rotated basis, the blue arrows are actual spiral spin orientations which only deviate slightly from the red arrows. The deviation angles increases as β increases in the 3×1 staircase. The spiral states at 4×1, 5×1 and other devil's staircases (not shown) can be similarly constructed. The inset show the spin axis for the collinear and spiral states. The degeneracy is $2N$ for odd N and N for even N. There is also a small magnetization for N odd, but exactly zero for N even. Bottom layer: the classically degenerate (2 in , 2 out) 2×2 vortex state along the diagonal line $\alpha = \beta$ is simply a FM state in the XY plane in the rotated basis $\tilde{\mathbf{S}}_n = R(\hat{x}, \pi n_1)R(\hat{y}, \pi n_2)\mathbf{S}_n$. The 3×3 skyrmion crystal (non-coplanar) state with non-vanishing skyrmion density $\vec{S}_i \cdot \vec{S}_j \times \vec{S}_k \neq 0$ happens near $\alpha = \beta = \pi/3$ which is the most frustrated regime in the Wilson loop[32]. Its detailed spin configuration is given in the Fig.S2 in the SM. The inset show the spin axis for the vortex and SkX states.

$\alpha = \beta = \pi/2$. At the classical level, the 2×1 Y-x stripy state $S^y = (-1)^x$ is degenerate with the 1×2 X-y stripy state $S^x = (-1)^y$. In fact, we find there is a family of states called 2×2 vortex states in Fig.2: $\mathbf{S}_i = ((-1)^{i_y}\cos\phi, (-1)^{i_x}\sin\phi, 0)$ which are degenerate at the classical level. In general, this family breaks the $C_4\times C_4$ symmetry except at $\phi = \pm\pi/4, \pm3\pi/4$. When $\phi = 0, \pi/2$, it recovers to the X-y and Y-x state respectively. Quantum fluctuations ("order from disorder" mechanism) are needed to find the unique quantum ground state upto the $C_4\times C_4$ symmetry in this regime. To perform a LSW calculation, one need to introduce a 4 sublattice structure A, B, C, D shown in Fig.2. After making suitable rotations to align the spin quantization axis along the Z axis, we introduce 4 HP bosons a, b, c, d to perform a systematic $1/S$ expansion shown in Eqn.3 where $E_0 = -2NJS^2(1-\cos2\alpha\sin^2\phi - \cos2\beta\cos^2\phi)$ is the classical ground state energy, H_2 can be diagonized by a unitary transformation, then followed by a Bogoli-

ubov transformation as:

$$H_2 = E_2 + 2\sum_{n,k} \omega_n(k)\alpha^\dagger_{n,k}\alpha_{n,k} \tag{9}$$

where $n = 1, 2, 3, 4$ is the sum over the 4 branches of spin wave spectrum in the Reduced BZ $-\pi/2 < k_x, k_y < \pi/2$ and E_2 is the $1/S$ quantum correction to the ground-state energy:

$$E_2 = \sum_{k,n}[\omega_n(k) - (1 - \cos 2\alpha \sin^2\phi - \cos 2\beta \cos^2\phi)/2] \tag{10}$$

Obviously, near the Abelian point $\alpha = \beta = \pi/2$, if $\alpha > \beta$, it picks the Y-x state with $\phi = \pi/2$. If $\alpha < \beta$, it picks the X-y state with $\phi = 0$. Setting $\alpha = \beta$, the $E_0 = -2NJS^2(1 - \cos 2\alpha)$ becomes ϕ independent, indicating the classical degenerate family of states characterized by the angle ϕ along the whole diagonal line $\alpha = \beta$. Fortunately, the quantum correction $E_2(\phi) = \sum_{k,n}[\omega_n(k, \phi) - \sin^2\alpha]$ does depend on ϕ. As shown in Fig.3a, we find that $E_2(\phi)$ reach its minimum at $\phi = 0$ (X-y state) or $\phi = \pi/2$ (Y-x state) which is related to each other by the $C_4 \times C_4$ symmetry. Expanding $E_2(\phi)$ (in unit of $2JS$) around one of its minima $\phi = 0$, $E_2(\phi) = E_2^0 + \frac{1}{2}B(\alpha)\phi^2 + \cdots$, one can identify the coefficient $B(\alpha)$ as plotted in the Fig.3b.

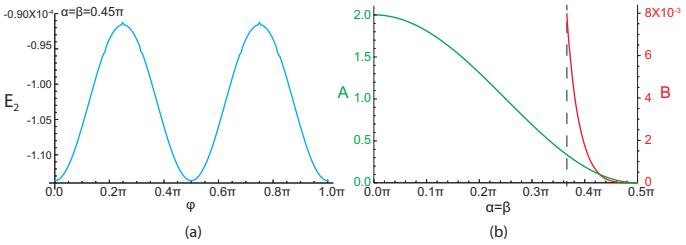

FIG. 3. The order from disorder and the gap opening on the spurious gapless mode along the diagonal line in Fig.1. (a) The quantum correction to the ground-state energy from the LSW. $\phi = 0$ corresponds to X-y state and $\phi = \pi/2$ corresponds to Y-x state. So the quantum fluctuations pick up Y-x or X-y as the ground state which is related to each other by the $C_4 \times C_4$ symmetry. (b) The classical coefficient $A(\alpha)/J$ and the quantum one $B(\alpha)/J$. Both vanish at the Abelian point $\alpha = \beta = \pi/2$ as $\sim (\pi/2 - \alpha)^2$ and are monotonically increasing function when moving away from the Abelian point. The Dashed line is located at $\alpha^0_{in} \sim 0.3661\pi$ where the Y-x state becomes unstable at the LSW order. After incorporating the gap opening, the α^0_{in} is shifted to a smaller value $\alpha_{in} \sim 0.3526\pi$.

The quantum order from disorder selection of the Y-x or X-y state along the diagonal line shows that there is a direct first order transition from the Y-x state to the X-y state along the diagonal line in Fig.1. So along the diagonal line, there is any mixture of the Y-x and X-y state. Similar first order transition between vacancy induced supersolid (SS-v) and interstitial induced supersolid (SS-i) and any mixtures of the two along the particle-hole symmetric line at the half filling in a triangular lattice were discussed in[40–42].

The magnon gap generated by the order from disorder mechanism. The gapless nature of the spin wave spectrum Eqn.8 is just a spurious fact of the LSW approximation. It will be gapped out by the higher order terms in the $1/S$ expansion Eqn.3. As shown in the next section, the quantum Lifshitz transition remains, but with a different dynamic exponent $z = 1$ than that $(z_x = 1, z_y = 2)$ got within the LSW. It turns out that the leading order corrections to the gap at the minimum $(\pi, 0)$ of the C-C_π magnons can be achieved by the spin coherent state path integral formulation[3,43]. A general uniform state at $\vec{q} = 0$ can be taken as a FM state with the polar angle (θ, ϕ) in the $\tilde{SU}(2)$ basis with $\vec{\tilde{S}}_i = R(\hat{x}, \pi n_1)R(\hat{y}, \pi n_2)\vec{S}_i$ at the $\alpha = \beta = \pi/2$ Abelian point. After transforming back to the original basis by using $\tilde{S}_1 = R_z(\pi)S_1$, $\tilde{S}_2 = R_y(\pi)S_2, \tilde{S}_3 = R_x(\pi)S_3, \tilde{S}_4 = S_4$, it leads to a 2×2 state characterized by the two angles θ and ϕ. Along the diagonal line, its classical energy becomes

$$H_0 = J[-2\sin^2\alpha - 2\cos^2\alpha \sin^2\theta] \tag{11}$$

which is, as expected, ϕ in-dependent. But one can see any deviation from the Abelian point picks up the XY plane with $\theta = \pi/2$. So it reduces to the 2×2 vortex state in Fig.2 used in the " order from disorder " analysis in the last section. Expanding around the minimum $H_0 = J[-2\sin^2\alpha + 2\cos^2\alpha(\theta - \frac{\pi}{2})^2 + \cdots]$ gives the stiffness $A = 2J\cos^2\alpha$ shown in Fig.3b. Using the spin coherent state analysis, we can write down the quantum spin action at $\vec{q} = 0$:

$$\mathcal{L}(\vec{q} = 0) = iS\cos\theta\partial_\tau\phi + \frac{1}{2}S^2A(\theta - \pi/2)^2 + \frac{1}{2}SB\phi^2 \tag{12}$$

where we put back the spin S, the first term is the spin Berry phase term, $A \sim (\pi/2 - \alpha)^2$ and $B \sim (\pi/2 - \alpha)^2$ are from the classical analysis in Eqn.11 and the quantum order from disorder analysis to LSW order in Eqn.10 respectively. Eqn.12 leads to the quantized Hamiltonian $H(\vec{q} = 0) = (a_0^\dagger a_0 + 1/2)\hbar\Delta_B$ with the gap $\Delta_B = \sqrt{SAB} \propto \sqrt{S}$. In fact, there are also corrections from the cubic H_3 and quartic H_4 terms in Eqn.3, but they only contribute to order of 1 which is subleading to the $\sqrt{S}$ order in the $1/S$ expansion[44,45]. As shown in Fig.3b, because both A and B are monotonically increasing along the diagonal line, so the gap also increase. Plugging their values at $\alpha = \alpha^0_{in} = \arccos(1/\sqrt{6})$, When taking $A/J = 1/3, B/J \approx 0.008$ and $S = 1/2$, we find the maximum gap near the quantum Lifshitz transition $\Delta_B/J \sim 0.036$.

Quantum Lifshitz transition from the Y-x (X-y) to IC-SkX/Y-x (IC-SkX/X-y) state. As shown in the last section, there is a gap Δ_B opening at $\vec{q} = 0$ along the diagonal line, so the quantum Lifshitz transition point will shift to a smaller value of α. Incorporating

the gap Δ_B into the spin-wave dispersion ω_k in Eqn.8 at the LSW order leads to $\Omega_q = \sqrt{\Delta_B^2 + \omega_q^2}$ (See the Methods). Because the spectrum along q_x is non-critical, so one can just put $q_x = 0$:

$$\omega_-(q_x = 0, q_y) = \sqrt{\Delta_B^2 + v_y^2 q_y^2 + u^2 q_y^4 + \cdots} \qquad (13)$$

where $v_y^2 = a(\alpha_{in}^0 - \alpha)$ changes sign at $\alpha = \alpha_{in}^0 \sim 0.3611\pi$ (Fig.4a). From the gap vanishing condition[46] at the IC wave-vectors $q_{ic} = \pm(\Delta_B/u)^{1/2}$, one can see the quantum Lifshitz transition is shifted to $\alpha_{ic} = \alpha_{in}^0 - 2u\Delta_B/a$. Plugging in the values of Δ_B and u, we find $q_{ic} \sim 0.18\pi$ (Fig.4d) and the shift is so small that $\alpha_{ic} \sim 0.3526\pi$ remains larger than $\alpha_{33} \sim 0.3402\pi$ (to be defined in the next section) as shown in Fig.1. So there must be an In-commensurate phase intervening between the Y-x state and the 3×3 state when $\alpha_{33} < \alpha < \alpha_{ic}$ in Fig.1. The transition from the Y-x to IC state is a quantum Lifshitz transition with the dynamic exponent $z = 1$ (Fig. S1d) instead of the one with $(z_x = 1, z_y = 2)$ at the LSW order in Fig.4a. The IC phase has the 4 orbital order wave-vectors $(0, \pm(\pi - q_y^0))$ and $(\pi, \pm(\pi - q_y^0))$ with $q_y^0 \geq q_{ic}$. The spin structure of this IC phase remains to be determined. It should be a non-coplanar IC Skyrmion crystal phase which we name as IC-SkX/Y-x phase. Similarly, starting form the X-y phase, one can reach the IC-SkX/X-y phase with the 4 orbital order wave-vectors $(\pm(\pi - q_x^0), 0)$ and $(\pm(\pi - q_x^0), \pi)$. The Y-x state has the C-C_π magnons when $\alpha_{in}^0 < \alpha < \pi/2$, the C-IC magnons at the two minima $(0, \pm k_y^0)$ with $\pi - q_{ic} < k_y^0 < \pi$ when $\alpha_{in} < \alpha < \alpha_{in}^0$ as shown in Fig.4c. So along the diagonal line $\alpha_{ic} < \alpha < \pi/2$ ($\alpha_{33} < \alpha < \alpha_{ic}$), there must be co-existence of the Y-x and X-y (IC-SkX/Y-x and IC-SkX/X-y) phases with any ratios (Fig.1 and its inset). This physical picture will be substantiated further from the anisotropic line $(\alpha = \pi/2, \beta)$ approached from the right.

Non-coplanar 3×3 Skyrmion Crystal phase and Co-planar spiral phases along the diagonal line $\alpha = \beta$.

1. 3×3 non-coplanar Skyrmion Crystal phase (SkX). Near $\alpha = \beta = \pi/3$, it is natural to take a 3×3 ansatz: $S_{(i_x, i_y)} = S_{(i_x + 3m, i_y + 3n)}$ with $m, n \in \mathbb{Z}$. We estimate its classical ground-state energy by minimizing $E_{3\times3}(\{\phi_i, \theta_i\}_{0 \leq i \leq 9})$ over its 18 variables. Along the diagonal line ($\alpha = \beta$), as long as α is not too small, the minimization of $E_{3\times3}$ always leads to a $C_4 \times C_4$ symmetric 3×3 SkX state (See SM) shown in Fig.2. This is in sharp contrast to the case near $\alpha = \beta = \pi/2$ where the classical analysis only leads to the degenerate family of 2×2 vortex states shown in Fig.2. A quantum " order from disorder " analysis is needed to show the 2×2 vortex state phase separates into any mixtures of the Y-x state and X-y state along the diagnose line.

Comparing the classical ground energy of the 3×3 SkX with that of the Y-x state $E_{Y-x} = -2J \sin^2 \alpha$ leads to a putative first order transition between the two states at $\alpha_{33} \approx 0.340188\pi$ which is smaller than $\alpha_{ic} \sim 0.3526\pi$. So a putative direct first order transition between the Y-x state and the 3×3 SkX splits into 2 second order quantum Lifshitz transitions with $z = 1$ with the IC-SkX intervening between them. In fact, α_{33} also shifts to a smaller value due to the intervening of the IC-SkX/Y-x phase, but for simplicity, we still use the same symbol. The point $\alpha = \alpha_{33}$ in Fig.1 is a bi-critical point. Similarly, by LSW, we can determine the excitations spectra above the 3×3 SkX. We expect the transition from the IC-SKY/Y-x state to the 3×3 SkX is also a quantum Lifshitz transition with $z = 1$.

2. The Y-x state to the IC-SkX/Y-x transition through the condensations of C-IC magnons As shown in the inset of Fig.1, approaching from the right in the Y-x phase, the crossing point between the $(0, \pm 2\pi/3)$ counter line of the Y-x phase and the C-IC condensation boundary just hits the corner of the 3×3 SkX crystal at the multicritical M point located at (α_M, β_M), so there is a Y-x to the IC-SkX/Y-x phase due to the condensations of C-IC magnons with the ordering wavevectors $\pi - \pi/3 < k_y^0 < \pi - 0.18\pi$. It leads to the non-coplanar IC-SkX/Y-x phase with the ordering wavevecrtors $(0, \pm k_y^0)$ and $(\pi, \pm k_y^0)$. This confirms the picture achieved along the diagonal line in the previous section. Putting $\alpha = \beta = \alpha_{33}$ into the formula for the constant contour at $(0, k_y^0)$ listed in the SM, one gets $k_y^0 \sim \pi - 0.24\pi$. So one can see that along the diagonal line $\alpha_{33} < \alpha < \alpha_{ic}$, the ordering wavevector of the IC-SkX/Y-x is $0.18\pi < q_y^0 < 0.24\pi$. While the transition from the 3×3 SkX to the IC-SkX/Y-x on the right is through the condensations of C-IC magnons with $0.24\pi < q_y^0 < \pi/3$. The non-coplanar IC-SkX/X-y phase with the ordering wavevecrtors $(\pm k_x^0, 0)$ and $(\pm k_x^0, \pi)$. is related to IC-SkX/Y-x by the $C_4 \times C_4$ rotation.

3. Co-planar spiral states near $\alpha = \beta = \pi/N$ and first order transition line. We find even at the classical level, there is a first order transition from the 4×1 state to the 1×4 state along the diagonal line (Fig.S2). While one need resorts " order from quantum disorder" mechanism to select out Y-x and X-y state as the quantum ground state near $\alpha = \pi/2$. This may be due to the fact that only near $\alpha = \pi/2$, the Y-x and X-y are collinear states and orthogonal to each other, while all the other commensurate states near $\alpha = \pi/N, N > 2$ are non-collinear (but co-planar in the YZ plane) spiral phases and not orthogonal to each other. It turns out the 3×3 SkX is the only commensurate non-coplanar state along the diagonal line (see SM). All the other phases separate into $N \times 1$ and $1 \times N$ co-planar spiral phase in the YZ plane. There are no stable C phases at $\alpha = \frac{\pi}{N} n$ with $n > 1$. However, as shown below, this kind of co-planar phases at $n > 1$ can be stable near the Abelian line $(0 < \alpha < \pi/2, \beta = 0)$.

Taking $N \to \infty$ limit, one may approach the $\alpha = \beta = 0$ Abelian point. It suggests some IC phase near the point. To test this prediction, we first identify a $U(1)$ family of degenerate classical state which is a FM state within XY plane. Then by performing a LSW on this degenerate manifold, the linear term indeed vanishes, but

the spin wave spectrum always become negative. This fact indicates the FM is always unstable, the true ground state should be some IC phases corresponding to $N \to \infty$ limit in the FK model.

Co-planar spiral phases at a small $0 < \beta < \alpha < \pi/2$ near the Abelian line, pre-empty of the magnon condensation transitions and the meta-stable Y-x phase.

1. Mapping to the one dimensional classical Frenkel-Kontorova (FK) Model at $S = \infty$. Now we try to understand the global phase diagram Fig.1 near the whole Abelian line at the bottom $0 < \alpha < \pi/2, \beta = 0$. We will establish the classical phase diagram by mapping its lower half $\beta < \alpha = \pi/N$ to the Frenkel-Kontorowa (FK) model with $N \times 1$ (stripe) ansatz. We consider a $N \times 1$ spin-orbital structure commensurate with a lattice with $N \times M$ lattice sites. We will reach the incommensurate limit by taking $N \to \infty$ limit. Within a general $N \times 1$ ansatz, applying the local spin rotation $\tilde{\mathbf{S}}_n = R(\hat{x}, 2\alpha n)\mathbf{S}_n$ in Eqn.2 to get rid of the R matrix along the x bonds, writing the spin as a classical unit vector in the rotated basis $\tilde{\mathbf{S}}_n = (\cos\tilde{\eta}_n, \sin\tilde{\xi}_n \sin\tilde{\eta}_n, \cos\tilde{\xi}_n \sin\tilde{\eta}_n)$, we find that any $\beta > 0$ picks up $\tilde{\eta}_n = \pi/2$ (namely, a coplanar state in $\tilde{Y}\tilde{Z}$ plane) and the trial energy per site is $E_{tri}(N\times 1) = -\frac{J}{N}\sum_{n=1}^{N}[\cos(\tilde{\xi}_n - \tilde{\xi}_{n+1}) - \sin^2\beta\cos(2\tilde{\xi}_n + 4\alpha n) + \cos^2\beta]$ which can be transformed back to the original frame using $\xi_n = \tilde{\xi}_n + 2n\alpha$ (so the spins remain in a coplanar state in the original YZ plane shown in Fig.2).

$$E_{FK} = -\frac{J}{N}\sum_{n=1}^{N}[\cos(\xi_{n+1} - \xi_n - 2\alpha) - \sin^2\beta\cos 2\xi_n + \cos^2\beta] \quad (14)$$

One can see that at a small β, by using $\cos(\xi_{n+1} - \xi_n - 2\alpha) \sim 1 - \frac{1}{2}(\xi_{n+1} - \xi_n - 2\alpha)^2$, $E_{tri}(N \times 1)$ maps to the 1d Frenkel-Kontorova (FK) Model discussed in[60] at a finite size N with the periodic boundary condition or 2d Pokrovsky-Talapov (PT) which was used to discuss C-IC transition in 2d Bilayer quantum Hall systems[61].

Some insights can be achieved from the FK model at a small β. The kinetic term favors $\xi_{n+1} = \xi_n + 2\alpha$, while the potential term favors $\xi_n = \pm\pi/2$. When $\alpha = \pi/2$, this leads to the Y-x state as the exact ground state. However, when $\alpha = \pi/N, N = 3, 4, 5, \cdots$, frustrations comes in. At a small β, the kinetic term dominates over the potential term, so $\xi_{n+1} \sim \xi_n + 2\alpha$ still holds approximately as shown for the $3 \times 1, 4 \times 1, 5 \times 1$ spiral state in Fig.2. There are qualitative even-odd differences: The net magnetization in the $N \times 1$ unit cell is small, but non-vanishing for odd N, exactly vanishes for even N. Even N always has a larger stable regime than its previous odd $N-1$. There is a always cyclic degeneracy N for both even and odd N. The $\mathcal{T}$ gives a different state for N odd, but not for even N. So the degeneracy is $2N$ for odd N, just N for even N. One can check other symmetries operations $\mathcal{P}_x, \mathcal{P}_y, \mathcal{P}_z$ do not generate new states.

2. The pre-empty of the magnon condensations by first order transitions in the Y-x phase For any parameter $\beta < \alpha = \pi/N$, Eq.(14) gives the best estimation of the ground-state energy as $\min_{N\in[1,\infty)} E_{N\times 1}$ which can be compared to that of the Y-x state $E_{Y-x} = -2J\sin^2\alpha$. If one finds $\min E_{N\times 1} < E_{Y-x}$ for some N, then it means Y-x becomes unstable against some stripe spiral IC phase. Note that even $\min E_{N\times 1}$ may not give real ground-state energy, but it does give a upper bound for the ground-state energy of the stripe spiral IC phase whose precise nature is difficult to determine using the $N \times 1$ ansatz in a finite size calculation. The first order transition line from the Y-x to some IC phases is drawn in Fig.1. It matches very precisely the line achieved from the previous works[34,35] using classical Monte-Carlo simulations. It also hits the $\pm 2\pi/3$ contour line inside the Y-x phase at one corner of the 3×3 SkX phase which is a multi-critical (M) point at $(\alpha_M, \beta_M) \approx (0.33952\pi, 0.31284\pi)$ of several commensurate and In-commensurate phases in Fig.1. So all the C-C_0 regime and the C-IC regime with $0 < k_y^0 < 2\pi/3$ in the Y-x phase are pre-emptied by some spiral IC phases through the first-order transition line. So the Y-x state becomes only a meta-stable state (just a local minimum in energy landscapes) between the first-order transition line and the putative 2nd-order condensation boundary of the C-C_0 and the C-IC magnons. So hysteresis behaviors are expected in this regime. There is no mirror symmetry anymore beyond the LSW. For example, the C-C_π regime at $\alpha = \beta$ entertains the gap opening process due to the quantum order from disorder phenomena. However, its mirror image which is the C-C_0 regime at $\alpha = \pi/2 - \beta$ in Eqn.7 sustains no such phenomena. Of course, the condensation boundary at $0 < \beta < \beta_M \sim 0.31284\pi$ suffers a small shift due to the higher order terms in Eqn.3. But it is completely pre-emptied by the first order transition anyway.

3. Co-planar spiral states near $\alpha = \frac{\pi}{N}n$. In contrast to the Y-x state near $\alpha = \pi/2$, the commensurate phases near $\alpha = \pi/3, \pi/4, \pi/5, \cdots$ are stripe co-planar (in the YZ plane) spiral phases shown in Fig.2 instead of a collinear phase. As shown in the last section, we also find stable co-planar spiral phase at $\alpha = \pi/N, N > 2$ along the diagonal line. So these phases found near the Abelian line $\beta \ll 1$ will extend all the way to the diagonal line $\alpha = \beta$. However, the co-planar phases for $n = 2, 3, \cdots, [N/2]$ will not survive to the diagonal line. It is straightforward to extend our calculations near $\alpha = \pi/2$ to near $\alpha = \frac{\pi}{N}n$ to determine the excitation spectra in these phases which are expected to take the same form as the 2×1 Y-x state derived in Eq.5: $E_-(q) = \sqrt{\Delta^2 + v_x^2 q_x^2 + v_y^2 q_y^2}$. As N gets bigger, Δ and v_y gets smaller, so the stability regimes (or the widths of the devil staircases) in Fig.1 gets smaller. At an IC phase, $\Delta \to 0$ and $v_y \to 0$, it becomes a gapless state which is responsible for its zero width in Fig.1. We expect it has the anisotropic dis-

persion $E(q) = \sqrt{v_x^2 q_x^2 + u^2 q_y^4}$ which may be called an anisotropic phason mode. Interesting, if this form is indeed correct, it takes a similar form as that of the lattice phonon mode in the LSDW+CDW which is one of the Itinerant magnetic phases in a three-dimensional repulsively interacting Fermi gas with Weyl type of spin-orbit coupling[39].

It is also interesting to determine the classical first order transition boundaries between these robust C phases at $\alpha = \frac{\pi}{N}$ with some IC phases achieved from the FK model Eq.14 and then to check if they will pre-empty the second order phase transitions due to the condensations of these magnons. If so, then these spiral phase become meta-stable between the first order transitions and their corresponding second order condensation boundaries just like the collinear Y-x state shown as dashed lines in Fig.1.

Rational and irrational topological winding numbers, In-complete and complete devil's staircases. From all the co-planar spiral phases in Fig.2, one can define the topological winding number $W = (\xi_N - \xi_0)/N$. For the C-phase at $\alpha = \pi/N$, $W/2\pi = 2\alpha/2\pi = 1/N$ is a rational winding number which is dependent of the intermediate values of $\xi_n, n = 0, 1, ..., N-1$. For the other C phases at $\alpha = \frac{\pi}{N}n$ with $n > 1$, the winding number is found to be $W/2\pi = 2\alpha/2\pi = \frac{n}{N}$. The quantum fluctuations will certainly reduce the magnitude of spin at a given site $\vec{M}_i = \langle \vec{S}_i \rangle$. However, as long as the $\vec{M}_i \neq 0$, one can still define the fractional winding number $W/2\pi$ in terms of its phase. So due to its topological features, the definition of the winding number $W/2\pi$ also hold in the quantum case. For an In-commensurate phase, one can still define $W = Lim_{N\to\infty}(\xi_N - \xi_0)/N$ which becomes an irrational number. Each C phase occupies a step with the length Δ_c, the total C length $L_c = \sum_{\{C\}} \Delta_c$, its ratio over the total length L_0 gives the measure of all the C phases L_c/L_0. For an in-complete devil staircases, $L_c/L_0 < 1$, the rest $1 - L_c/L_0 > 0$ goes to the measure of the IC phases. For a complete devil staircases, $L_c/L_0 = 1$, while the IC phases intervening the C phases become a set of measure zero. For a harmless devil staircases, there is a direct first order transition between the two C phases with no intervening IC phases.

1. In-complete devil's staircases near the Abelian line. Near the Abelian line $\beta \ll 1$, Eq.14 can be mapped to the FK model in the weak locking regime. As shown in Fig.1, in addition to the $N\times 1$ C phase, the C phases at $\alpha = \frac{\pi}{N}n$ with $n > 1$ also contribute to $L_c = \sum_{\{C\}} \Delta_c$. The total length $L_0 = 1/2 - \beta/\pi$. The C measure $L_c/L_0 < 1$, the IC measure $1 - L_c/L_0 > 0$. We expect that there are two following limiting cases in Fig.1: As $\beta \to 0$ approaches the Abelian line, $L_c/L_0 \to 0, 1 - L_c/L_0 \to 1^-$, so the IC phases takes almost all the measures. As β approaches the diagonal line, $L_c/L_0 \to 1^-, 1 - L_c/L_0 \to 0^+$, the C phases takes almost all the measures. At the transition point $\alpha = \beta$, it just becomes the complete devil staircases where the IC phases take the Cantor set with a fractal dimension.

2. Complete devil's staircases along the diagonal line. Near the diagonal line $\alpha = \beta$, the mapping to the FK model may not be precise anymore. Along the diagonal line, as shown in Fig.1, only the $N \times 1$ C phase occupies a step with the length $\Delta_{N\times 1}$, the total C length $L_C = \sum_{N=4}^{\infty} \Delta_{N\times 1}$ and the total length $L_0 = \alpha_{4\times 1} \sim 0.295\pi$. As shown in the appendix, the $N \times 1, N \geq 4$ (or $1 \times N$) forms a complete devil staircases instead of a harmless one. In fact, as speculated above, they just lie at the transition point from the in-complete devil staircases below the diagonal line to the complete ones along the diagonal line, so the IC phases form a Cantor set with a non-integer fractal dimension.

Implications on cold atom experiments and materials with SOC. The orbital ordering wavevectors in all the phases in Fig.1 have been listed in the SM. As said below Eq.2, there is no spin-orbital coupled $U(1)$ symmetry away from the line $(\alpha = \pi/2, \beta)$, so one need to calculate the 3×3 tensor $\langle S_i(\vec{k}, \omega) S_j(-\vec{k}, -\omega)\rangle$. Following[32], one can work out the thermodynamic quantities such as magnetization, uniform and staggered susceptibilities, specific heat at the low temperatures in all the phases in Fig.1. Similarly, one can work out various kinds of spin correlation functions at the low and high temperatures. In the cold atom contexts, all these physical quantities can be detected by atom or light Bragg spectroscopies[49,50], specific heat measurements[51,52] and the *In-Situ* measurements[53]. In materials, they can be easily measured by magnetic resonant X-ray diffraction or neutron scattering techniques[55–57].

There have been some remarkable experimental advances to generate various kinds of 2D SOC for cold atoms in both continuum and optical lattices. A 2d Rashba SOC was implemented by Raman scheme in the fermion ^{40}K gas[23,24]. Using an optical Raman lattice scheme, Wu *et al*[25] realized the tunable quantum Anomalous Hall (QAH) SOC of spinor bosons ^{87}Rb in a square lattice. More recently, the fermionic optical lattice clock[26] scheme was successfully implemented to generate a strong SOC for ^{87}Sr clock[27], ^{173}Yb clock[28] and also ^{87}Rb[29], where the heating and atom loss from spontaneous emissions are eliminated, the exceptionally long lifetime $\sim 100s$ of the excited clock state have been achieved. In parallel, by using the most magnetic fermionic element dysprosium to eliminate the heating due to the spontaneous emission, the authors in[30] created a long-lived SOC gas of quantum degenerate atoms. The long lifetime of this weakly interacting SOC degenerate Fermi gas will also facilitate the experimental study of quantum many-body phenomena manifest at longer time scales. These ground-breaking experiments set-up a very promising platform to observe novel many-body phenomena shown in Fig.1 due to interplay between SOC and interaction in optical lattices.

Naively, due to its microscopic bosonic nature, the RFHM Eq.2 may not be useful to describe the magnetism in so called Kitaev materials such as Iridates or Osmates[5]. However, as shown in[32], the RFHM

can be expanded as Heisenberg- ferromagnetic Kitaev[36]-Dzyaloshinskii-Moriya (DM)[37] form with a dominant FM Kitave term which is indeed the case in these materials. Of course, the FM Kitave sign in these materials originates from the Hunds rules instead of the spinor bosonic nature of the underlying microscopic models.

In the so called 5d Kitaev materials such A_2IrO_3 with $A = Na_2, Li_2$ or more recent 4d materials $\alpha - RuCl_3$, so far, only Zig-Zag phase or an IC-SkX phase were observed experimentally[55–57], no spin liquids have been found. For example, an IC-SkX phase with the ordering wavevector $\vec{q} = (0, 0, q), q = \pi + \delta, \delta \sim 0.14\pi$ lying along the orthorhombic $\vec{a}$ axis was also detected on 3d hyperhoneycomb iridates α, β, γ-Li_2IrO_3 by resonant magnetic X-ray diffractions[55–57]. As shown in[32], the RFHM can be written as the Heisenberg- ferromagnetic Kitaev-DM form. One can estimate their separate numerical values near $\alpha = \alpha^0_{in} = \arccos\frac{1}{\sqrt{6}}$ in the IC-SkX with the ordering wavevectors $(0, \pm(\pi - q^0_y))$ and $(\pi, \pm(\pi - q^0_y))$ with $0.18\pi < q^0_y < \pi/3$ in the inset of Fig.1: the Heisenberg interaction $J^x_H = J^y_H \sim \cos 2\alpha = -2/3$, so it is an AFM coupling, the Ferromagnetic Kitaev interaction $J^x_K = J^y_K = 2\sin^2\alpha \sim 5/3$, the DM term $J^x_D = J^y_D = 2\sin 2\alpha \sim \sqrt{5}/3$. So the model becomes a dominant FM Kitaev term plus a small AFM Heisenberg term and a small DM term. So the RFHM could be an alternative minimal model to the Heisenberg-Kitaev-Ising (J, K, I) model used in[56,57] or Heisenberg-Kitaev-Exchange (J, K, Γ) model used in[58,59] to fit the experimental data phenomenologically. One common thing among all the three models is a dominant FM Kitaev term plus a small AFM Heisenberg term. It was known that there is no such IC-SkX phase in the Heisenberg-Kitaev model with only (J, K) term.

Various IC-SkX phase have also been observed in some helical magnets with a strong Dzyaloshinskii-Moriya (DM) interaction[37]. Indeed, a 2D skyrmion lattice has been observed between $h_{c1} = 50$ mT and $h_{c2} = 70$ mT in some chiral magnets MnSi or a thin film of $Fe_{0.5}Co_{0.5}Si$[54].

DISCUSSIONS

The order from disorder phenomena at the Rashba limit $\alpha = \beta$ in the range $\alpha_{33} \sim 0.34\pi < \alpha < 0.5\pi$ is due to the Rashba SOC which is a completely different mechanism than that due to the geometric frustrations[2–5]. The collinear spin-orbital coupled magnetic phase, the 3×3 SkX and the IC-SkX, stripe co-planar C and IC phases in Fig.1 can be contrasted to collinear and co-planar phases in geometrically frustrated magnets[1–4]. It was also speculated strong geometric fluctuations may lead to possible quantum spin liquids[5]. In fact, the SOC could be a new mechanism leading to new classes of quantum spin liquids which may have a good chance to be sandwiched by two commensurate magnetic phases. For example, the non-coplanar IC-SkX and co-planar IC phases in Fig.1 are particularly vulnerable to some small parameter changes. So it would be important to study if a spin liquid phase can creep in a honeycomb lattice with three SOC parameters (α, β, γ) putting on its three bonds. For example, it is tempting to see if the two kinds of IC phases will be fractionized into chiral spin liquids or spin liquids under the third SOC parameter γ in a honeycomb lattice. Indeed, there remains unknown deep connections among the in-commensurability, the hierarchy structures of fractals, spin liquids and their fractionalized excitations.

The strong correlations and quenched disorders lead to a new class of state of matter: quantum spin glass[6–9]. The multiple local (meta-stable) states, hysteresis and multi-fractals in Fig.1 may resemble the complex multiple local minimum landscapes in quantum spin glass. However, the former is SOC induced, the latter is due to quenched disorders. So the SOC may induce some similar complex glassy phenomena as the disorders do. Indeed, the non-coplanar IC-SkX phase and the coplanar IC phase in Fig.1 completely breaks the translational symmetry along the y axis and the x axis respectively. The possible connections between the quantum fluctuations in the multi-fractals in Fig.1 and the quantum chaos in the quantum spin glass deserve to be explored further[6–13].

In this paper, we only discussed the spinor bosons. Starting from the results achieved in both weak and strong coupling along the anisotropic line $(\alpha = \pi/2, \beta)$ in the fermionic case[48], we will map out the global quantum phase diagram for spin 1/2 fermion case in the generic (α, β) SOC parameter space in both weak and strong coupling limits. We may also explore the quantum or topological transitions between the two limits.

METHODS

In the main text, by the spin-coherent state path integral, we obtained the gap opening in the Y-x state along the diagonal $\tilde{\Delta}_B = J\sqrt{SAB} = 4JS\sqrt{AB/(16S)} = 4JS\Delta_B$. Note that in Eqn.3, the unit of spin wave dispersion at the LSW order is in the unit of $4JS$. Incorporating the gap Δ_B into the spin-wave dispersion ω_k in Eqn.8 at the LSW order leads to $\Omega_q = \sqrt{\Delta^2_B + \omega^2_q}$ whose evolution is shown in Fig.4 (because $B \ll A$ as shown in Fig.3b, so we ignore its small contribution to ω_q). Plugging in the value of the gap $\Delta_B \sim 0.036$, we estimate the new quantum critical point is shifted to $\alpha = \alpha_{in} = 0.3526\pi$ with the onset orbital order $q_{ic} \sim 0.18\pi$ as shown in Fig.4d. This is a quantum Lifshitz C-IC transition from the Y-x state to the IC-SkX/Y-x with the dynamic exponent $z = 1$.

Because the IC-SkX/Y-x phase has the 4 orbital ordering wave-vectors $(0, \pm(\pi - q^0_y))$ and $(\pi, \pm(\pi - q^0_y))$, the most general spin structures for the two transverse components can be written as:

$$S^x(x, y) = [A + B(-1)^x]e^{i(\pi - q^0_y)y} + h.c$$
$$S^z(x, y) = [C + D(-1)^x]e^{i(\pi - q^0_y)y} + h.c \qquad (15)$$

where $q_{ic} \sim 0.18\pi < q^0_y < 0.24\pi$.

The longitudinal component $S^y(x, y)$ can also be written as:

$$S^y(x, y) = [E + F(-1)^x]e^{i(\pi - q^0_y)y} + h.c \qquad (16)$$

The 6 complex numbers A, B, C, D and E, F should satisfy the classical constraint $\sum_{\alpha=1}^{3} S_\alpha^2 = S^2$. at any IC momentum q_y^0. These parameters can be determined by the minimization of the classical energy of the IC-SkX Eqn.15 in the range $\alpha_{33} < \alpha < \alpha_{in}$ along the diagonal line.

As shown in the main text, there is also a transition from the Y-x state to the IC-SkX/Y-x from the Y-x state on the right due to the condensations of the C-IC magnons with $\pi - \pi/3 < k_y^0 < \pi - 0.18\pi$ (or equivalently $0.18\pi < q_y^0 < \pi/3$).

Eq.15 can also be written as $S_\alpha = Re[(\psi_{1\alpha} + \psi_{2\alpha}(-1)^x)e^{i(\pi - q_y^0)y}]$ where $\alpha = x, z$ stands for the two transverse components. It is interesting to construct a GL action in terms of the order parameters $\psi_{a\alpha}, a = 1, 2, \alpha = x, z$ to describe the quantum Lifshitz transition. Note that although the IC-SkX/Y-x phase in Eq.15 breaks the crystal translational symmetry along the x axis only to two sites per unit cell, it completely breaks the crystal translational symmetry along the y axis. It is infinitely degenerate, but discrete and countable. So its excitation spectrum should still have a gap. Because the crystal momentum k_y is not a good quantum number anymore, so there maybe dis-commensurations or domain walls along the y axis. It remains interesting to determine the distributions of these dis-commensurations and their repulsive interactions in the IC-SKX phases.

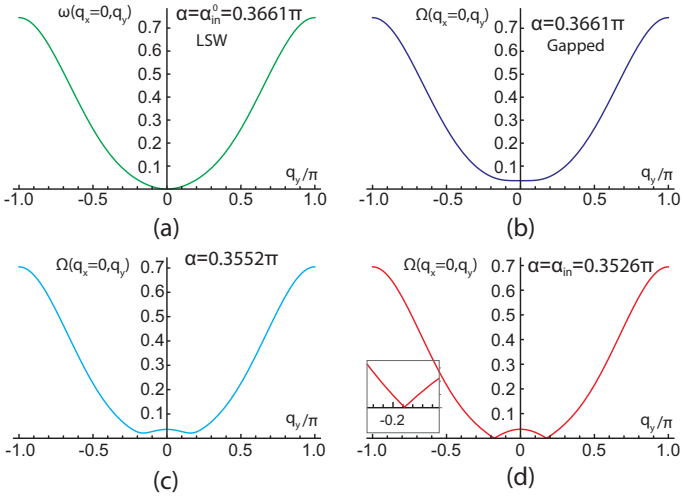

FIG. 4. The quantum Lifshitz C-IC transition from the Y-x state to the IC-SkX/Y-x state along the diagonal line $\alpha = \beta$. The momentum is expanded near $\vec{k} = (0, \pi) + \vec{q}$. (a) The transition happens at $\alpha = \alpha_{\rm in}^0 = 0.3661\pi$ at the LSW order with the dynamic exponent $(z_x = 1, z_y = 2)$. (b) Order from disorder mechanism generates a gap Δ_B to the spin wave spectrum at $\alpha = \alpha_{\rm in}^0 = 0.3661\pi$. (c) As α decreases further, the Y-x state supports the C-IC magnons at $(0, k_y^0)$. (d) The C-IC transition due to the condensations of the C-IC magnons happens at $\alpha = \alpha_{\rm in} = 0.3552\pi$ with the onset in-commensurate order $q_{ic} = \pm(\Delta_B/u)^{1/2} \sim 0.18\pi$ and the dynamic exponent $(z_x = 1, z_y = 1)$ as shown in the inset.

SUPPLEMENTARY MATERIALS

Supplementary materials for this article is available at http://advances.sciencemag.org/

[1] A. V. Chubukov, S. Sachdev, and J. Ye, *Theory of two-dimensional quantum Heisenberg antiferromagnets with a nearly critical ground state*, Phys. Rev. B **49**, 11919(1994).

[2] S. Sachdev, *Quantum Phase transitions*, (2nd edition, Cambridge University Press, 2011).

[3] A. Auerbach, *Interacting electrons and quantum magnetism*, (Springer Science & Business Media, 1994).

[4] B.I. Halperin and W.M. Saslow, Phys. Rev. B 16, 2154 (1977).

[5] L. Savary and L. Balents, *Quantum Spin liquids*, arXiv:1601.03742 (2016).

[6] J. Ye, S. Sachdev and N. Read, A solvable spin glass of quantum rotors, Phys. Rev. Lett. 70, 4011 (1993)

[7] S. Sachdev and J. Ye, Gapless spin-fluid ground state in a random quantum Heisenberg magnet, Phys. Rev. Lett. 70, 3339 (1993)

[8] N. Read, S. Sachdev and J. Ye, Landau theory of quantum spin glasses of rotors and Ising spins, Phys.Rev.B,52, 384 (1995

[9] Yi-Zhuang You, Andreas W. W. Ludwig, Cenke Xu, Sachdev-Ye-Kitaev Model and Thermalization on the Boundary of Many-Body Localized Fermionic Symmetry

Protected Topological States, arXiv:1602.06964
[10] Subir Sachdev, Holographic Metals and the Fractionalized Fermi Liquid, Phys. Rev. Lett. 105, 151602 C Published 4 October 2010.
[11] A. Kitaev, A simple model of quantum holography," KITP strings seminar and Entanglement 2015 program (Feb. 12, April 7, and May 27, 2015) . http://online.kitp.ucsb.edu/online/entangled15/.
[12] Joseph Polchinski, Vladimir Rosenhaus, The Spectrum in the Sachdev-Ye-Kitaev Model, arXiv:1601.06768.
[13] Antal Jevicki, Kenta Suzuki, Junggi Yoon, Bi-Local Holography in the SYK Model, arXiv:1603.06246.
[14] Juan Maldacena, Douglas Stanford, Comments on the Sachdev-Ye-Kitaev model, arXiv:1604.07818.
[15] Y. A. Bychkov and E.I. Rashba, Oscillatory effects and the magnetic susceptibility of carriers in inversion layers, J. Phys. C 17, 6039 (1984).
[16] Jinwu Ye, Yong Baek Kim, A. J. Millis, B. I. Shraiman, P. Majumdar, and Z. Tesanovic Berry phase theory of the Anomalous Hall Effect: Application to Colossal Magnetoresistance Manganites, Phys. Rev. Lett. 83, 3737 (1999)
[17] Lev P. Gor'kov and Emmanuel I. Rashba, Superconducting 2D System with Lifted Spin Degeneracy: Mixed Singlet-Triplet State, Phys. Rev. Lett. 87, 037004 (2001).
[18] T. Jungwirth, Qian Niu and A. H. MacDonald, Anomalous Hall Effect in Ferromagnetic Semiconductors, Phys. Rev. Lett. 88, 207208 (2004).
[19] Jairo Sinova, Dimitrie Culcer, Q. Niu, N. A. Sinitsyn, T. Jungwirth, and A. H. MacDonald, Universal intrinsic spin Hall effect, Phys. Rev. Lett. 92, 126603 (2004).
[20] Wang Yao and Qian Niu, Berry Phase Effect on the Exciton Transport and on the Exciton Bose-Einstein Condensate, Phys. Rev. Lett. 101, 106401 (2008).
[21] Naoto Nagaosa, Jairo Sinova, Shigeki Onoda, A. H. MacDonald, and N. P. Ong, Anomalous Hall effect, Rev. Mod. Phys. 82, 1539 (2010) - Published 13 May 2010.
[22] Jairo Sinova, Sergio O. Valenzuela, J. Wunderlich, C.?H. Back, and T. Jungwirth, Spin Hall effects, Rev. Mod. Phys. 87, 1213 (2015) - Published 27 October 2015
[23] Lianghui Huang, *et.al*, Experimental realization of a two-dimensional synthetic spin-orbit coupling in ultracold Fermi gases, arXiv:1506.02861. To appear in Nature Physics.
[24] Zengming Meng, *et.al*, Experimental observation of topological band gap opening in ultracold Fermi gases with two-dimensional spin-orbit coupling, arXiv:1511.08492.
[25] Zhan Wu, *et.al*, Realization of Two-Dimensional Spin-orbit Coupling for Bose-Einstein Condensates, arXiv:1511.08170
[26] Michael L. Wall, *et.al*, Synthetic Spin-Orbit Coupling in an Optical Lattice Clock, Phys. Rev. Lett. 116, 035301 (2016).
[27] L. F. Livi, G. Cappellini, M. Diem, L. Franchi, C. Clivati, M. Frittelli, F. Levi, D. Calonico, J. Catani, M. Inguscio, L. Fallani, Synthetic dimensions and spin-orbit coupling with an optical clock transition, Phys. Rev. Lett. 117, 220401 C Published 23 November 2016. Editors' Suggestion.
[28] S. Kolkowitz, S.L. Bromley, T. Bothwell, M.L. Wall, G.E. Marti, A.P. Koller, X. Zhang, A.M. Rey, J. Ye, Spin-orbit coupled fermions in an optical lattice clock, arXiv:1608.03854.
[29] Fangzhao Alex An, Eric J. Meier, Bryce Gadway, Direct observation of chiral currents and magnetic reflection in atomic flux lattices, arXiv:1609.09467.
[30] Nathaniel Q. Burdick, Yijun Tang, and Benjamin L. Lev, Long-Lived Spin-Orbit-Coupled Degenerate Dipolar Fermi Gas, Phys. Rev. X 6, 031022 C Published 17 August 2016.
[31] J. Dalibard, F. Gerbier, G. Juzeliūnas, and P. Öhberg, *Colloquium: Artificial gauge potentials for neutral atoms*, Rev. Mod. Phys. **83**, 1523 (2011).
[32] Fadi Sun, Jinwu Ye, Wu-Ming Liu, Quantum magnetism of spinor bosons in optical lattices with synthetic non-Abelian gauge fields at zero and finite temperatures, Phys. Rev. A 92, 043609 (2015).
[33] Zi Cai, Xiangfa Zhou, and Congjun Wu, Magnetic phases of bosons with synthetic spin-orbit coupling in optical lattices, Phys. Rev. A 85, 061605(R) C Published 20 June 2012
[34] J. Radić, A. Di Ciolo, K. Sun, and V. Galitski, *Exotic Quantum Spin Models in Spin-Orbit-Coupled Mott Insulators*, Phys. Rev. Lett. **109**, 085303 (2012).
[35] W. S. Cole, S. Zhang, A. Paramekanti, and N. Trivedi, *Bose-Hubbard Models with Synthetic Spin-Orbit Coupling: Mott Insulators, Spin Textures, and Superfluidity*, Phys. Rev. Lett. **109**, 085302 (2012).
[36] A. Kitaev, *Anyons in an exactly solved model and beyond. In the context of the present paper, the difference between honeycomb and a square lattice is not essential*, Ann. Phys. **321**, 2 (2006).
[37] I. Dzyaloshinskii, J. Phys. Chem. Solids **4**, 241 (1958); T. Moriya, Phys. Rev. **120**, 91 (1960).
[38] Fadi Sun, Jinwu Ye, Wu-Ming Liu, Classification of magnons in Rotated Ferromagnetic Heisenberg model and their competing responses in transverse fields, Phys. Rev. B 94, 024409 (2016).
[39] Shang-Shun Zhang, Jinwu Ye, Wu-Ming Liu, Itinerant magnetic phases and Quantum Lifshitz transitions in repulsively interacting spin-orbit coupled Fermi gas, Phys. Rev. B 94, 115121 (2016).
[40] Ye, J. Duality, magnetic space group and their applications to quantum phases and phase transitions on bipartite lattices in several experimental systems. *Nucl. Phys. B* **805**, 418 (2008).
[41] Chen, Y. & Ye, J., Characterizing boson orders in lattices by vortex degree of freedoms. *Philos. Mag.* **92**, 4484-4491 (2012).
[42] Ye, J. & Chen, Y. Quantum phases, Supersolids and quantum phase transitions of interacting bosons in frustrated lattices. *Nucl. Phys. B* **869**, 242 (2013).
[43] Murthy, G., Arovas, D. & Auerbach, A. Superfluids and supersolids on frustrated two-dimensional lattices. *Phys. Rev. B* **55**, 3104 (1997).
[44] R. T. Scalettar, G. G. Batrouni, A. P. Kampf, and G. T. Zimanyi, *Simultaneous diagonal and off-diagonal order in the Bose-Hubbard Hamiltonian*, Phys. Rev. B **51**, 8467 (1995).
[45] Jun-ichi Igarashi, 1/S expansion for thermodynamic quantities in a two-dimensional Heisenberg antiferromagnet at zero temperature, Phys. Rev. B 46, 10763C10771 (1992); Jun-ichi Igarashi and Tatsuya Nagao, 1MS-expansion study of spin waves in a two-dimensional Heisenberg antiferromagnet, Phys. Rev. B 72, 014403 (2005).
[46] For a classical bosonic Lifshitz type of transitions, see: Longhua Jiang and Jinwu Ye, Lattice structures of Larkin-Ovchinnikov-Fulde - Ferrell (LOFF) state, Phys. Rev. B 76, 184104 (2007).
[47] For scaling functions with the anisotropic dynamic exponents ($z_x = 2, z_y = 1$) where q_x is the colliding direction across a fermionic Lifshitz type of transitions, see F.

Sun, X.-L. Yu, J. Ye, H. Fan, and W.-M. Liu, *Topological Quantum Phase Transition in Synthetic Non-Abelian Gauge Potential: Gauge Invariance and Experimental Detections*, Sci. Rep. **3**, 2119 (2013).

[48] Fadi Sun, Jinwu Ye, Wu-Ming Liu, Hubbard model with Rashba or Dresselhaus spin-orbit coupling and Rotated Anti-ferromagnetic Heisenberg Model, arXiv:1601.01642

[49] J. Ye, J. M. Zhang, W. M. Liu, K. Zhang, Y. Li, and W. Zhang *Light-scattering detection of quantum phases of ultracold atoms in optical lattices*, Phys. Rev. A **83**, 051604 (2011).

[50] J. Ye, K. Y. Zhang, Y. Li, Y. Chen, and W. P. Zhang, *Optical Bragg, atom Bragg and cavity QED detections of quantum phases and excitation spectra of ultracold atoms in bipartite and frustrated optical lattices*, Ann. Phys. **328**, 103 (2013).

[51] J. Kinast, A. Turlapov, J. E. Thomas, Q. Chen, J. Stajic, and K. Levin, *Heat Capacity of a Strongly Interacting Fermi Gas*, Science **307**, 1296 (2005).

[52] M. J. H. Ku, A. T. Sommer, L. W. Cheuk, and M. W. Zwierlein, *Revealing the Superfluid Lambda Transition in the Universal Thermodynamics of a Unitary Fermi Gas*, Science **335**, 563 (2012).

[53] N.Gemelke, X. Zhang, C. L. Huang, and C. Chin, *In situ observation of incompressible Mott-insulating domains in ultracold atomic gases*, Nature (London) **460**, 995 (2009).

[54] X. Z. Yu, Y. Onose, N. Kanazawa, J. H. Park, J. H. Han, Y. Matsui, N. Nagaosa and Y. Tokura, Real-space observation of a two-dimensional skyrmion crystal, Nature 465,901C904(17 June 2010).

[55] A. Biffin, *et.al*, Noncoplanar and Counterrotating Incommensurate Magnetic Order Stabilized by Kitaev Interactions in Li 2 IrO 3, Phys. Rev. Lett. 113, 197201

[56] A. Biffin, *et. al* , Unconventional magnetic order on the hyperhoneycomb Kitaev lattice in ?Li2IrO3: Full solution via magnetic resonant x-ray diffraction, Phys. Rev. B 90, 205116 (2014)

[57] Itamar Kimchi, Radu Coldea, and Ashvin Vishwanath, Unified theory of spiral magnetism in the harmonic-honeycomb iridates , and Li 2 IrO 3, Phys. Rev. B 91, 245134 (2015).

[58] Jeffrey G. Rau, Eric Kin-Ho Lee, and Hae-Young Kee, Generic Spin Model for the Honeycomb Iridates beyond the Kitaev Limit, Phys. Rev. Lett. 112, 077204 (2014)

[59] Eric Kin-Ho Lee and Yong Baek Kim, Theory of magnetic phase diagrams in hyperhoneycomb and harmonic-honeycomb iridates, Phys. Rev. B 91, 064407 (2015).

[60] P. M. Chaikin and T. C. Lubensky principles of condensed matter physics(Cambridge university press,1995.)

[61] For areview on a bilayer quantum Hall systems, see S. M. Girvin and A. H. Macdonald, in Persepctives in Quantum Hall effects, edited by S. Das Sarma and Aron Pinczuk (Wiley, new York, 1997).

Acknowledgements

We thank W. M. Liu for encouragements and AFOSR FA9550-16-1-0412 for supports. The work at KITP was supported by NSF PHY11-25915.

Author Contributions

F. S and J. Y did the calculations. F. S wrote the notes leading to the manuscript. J.Y. designed this work and wrote the manuscript based on the notes. Both reviewed the manuscript.

Competing Interests: The authors declare no competing financial interests.

Correspondence: Correspondence and requests for materials should be addressed to Jinwu Ye at jy306@msstate.edu